ACCOUNTS of chemical research

Article

pubs.acs.org/accounts

From Nonfinite to Finite 1D Arrays of Origami Tiles

Tsai Chin Wu, Masudur Rahman, and Michael L. Norton*

Department of Chemistry, Marshall University, 1 John Marshall Drive, Huntingon, West Virginia 25755, United States

CONSPECTUS: DNA based nanotechnology provides a basis for high-resolution fabrication of objects almost without physical size limitations. However, the pathway to large-scale production of large objects is currently unclear. Operationally, one method forward is to use high information content, large building blocks, which can be generated with high yield and reproducibility. Although flat DNA origami naturally invites comparison to pixels in zero, one, and two dimensions and voxels in three dimensions and has provided an excellent mechanism for generating blocks of significant size and complexity and a multitude of shapes, the field is young enough that a single "brick" has not become the standard platform used by the majority of researchers in the field.

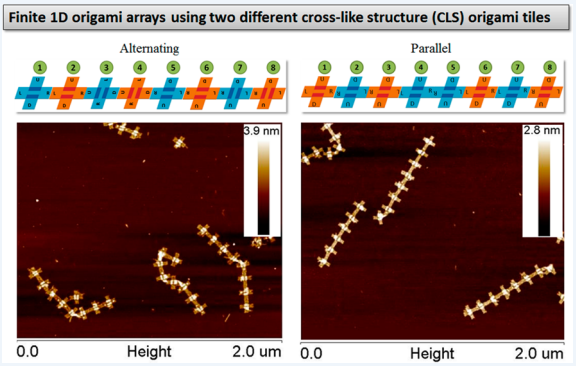

In this Account, we highlight factors we considered that led to our adoption of a cross-shaped, non-space-filling origami species, designed by Dr. Liu of the Seeman laboratory, as the building block ideal for use in the fabrication of finite one-dimensional arrays. Three approaches that can be employed for uniquely coding origami−origami linkages are presented. Such coding not only provides the energetics for tethering the species but also uniquely designates the relative orientation of the origami building blocks. The strength of the coding approach implemented in our laboratory is demonstrated using examples of oligomers ranging from finite multimers composed of four, six, and eight origami structures to semi-infinite polymers (100mers). Two approaches to finite array design and the series of assembly steps that each requires are discussed.

The process of AFM observation for array characterization is presented as a critical case study. For these soft species, the array images do not simply present the solution phase geometry projected onto a two-dimensional surface. There are additional perturbations associated with fluidic forces associated with sample preparation. At this time, reconstruction of the "true" or average solution structures for blocks is more readily achieved using computer models than using direct imaging methods.

The development of scalable 1D-origami arrays composed of uniquely addressable components is a logical, if not necessary, step in the evolution of higher order fully addressable structures. Our research into the fabrication of arrays has led us to generate a listing of several important areas of future endeavor. Of high importance is the re-enforcement of the mechanical properties of the building blocks and the organization of multiple arrays on a surface of technological importance. While addressing this short list of barriers to progress will prove challenging, coherent development along each of these lines of inquiry will accelerate the appearance of commercial scale molecular manufacturing.

1. INTRODUCTION

1.1. The Motivation for Large Nanostructures

One can see a point of divergence in the area of DNA nanotechnology,[1−3] one direction in which small, finite structures are the objective and another domain in which large objects are to be created.[4] At present, pharmaceuticals are perhaps the best example of the small nanostructure track.[4−10] For these systems, size constraints are imposed by the application space, biological systems, which have intrinsic pore and vesicle sizes. This domain contrasts strongly with the optoelectronic application domain, where the optimal size domain is perhaps bounded on the low side at 1 μm and the desired large-scale limit seems at this point to be undefined. The value of producing structures at least on the size scale of a micrometer on an edge is that such objects, if they could be positioned, would invite electrical connection to the larger world through "top down" lithography at a size scale that is accessible to large numbers of researchers.[11−15] While this 1 μm^2 scale would most likely not present commercially viable components, complex systems displaying the equivalent performance of 100−1000 modular, discrete, or individual components would invite prototyping efforts by a larger fraction of the electronics engineering community.[16]

1.2. Why Pursue 1D

One-dimensional arrayed systems represent the first departure from the single or discrete motif development path. There are two major drivers for the development of one-dimensional systems, quality control and expandability.

1.3. Assembly Diagnostics

One-dimensional systems promise to fulfill the need for platforms that enable the quantitation of assembly yield

Special Issue: Nucleic Acid Nanotechnology

Received: December 31, 2013
Published: May 6, 2014

   dx.doi.org/10.1021/ar400330y | Acc. Chem. Res. 2014, 47, 1750−1758

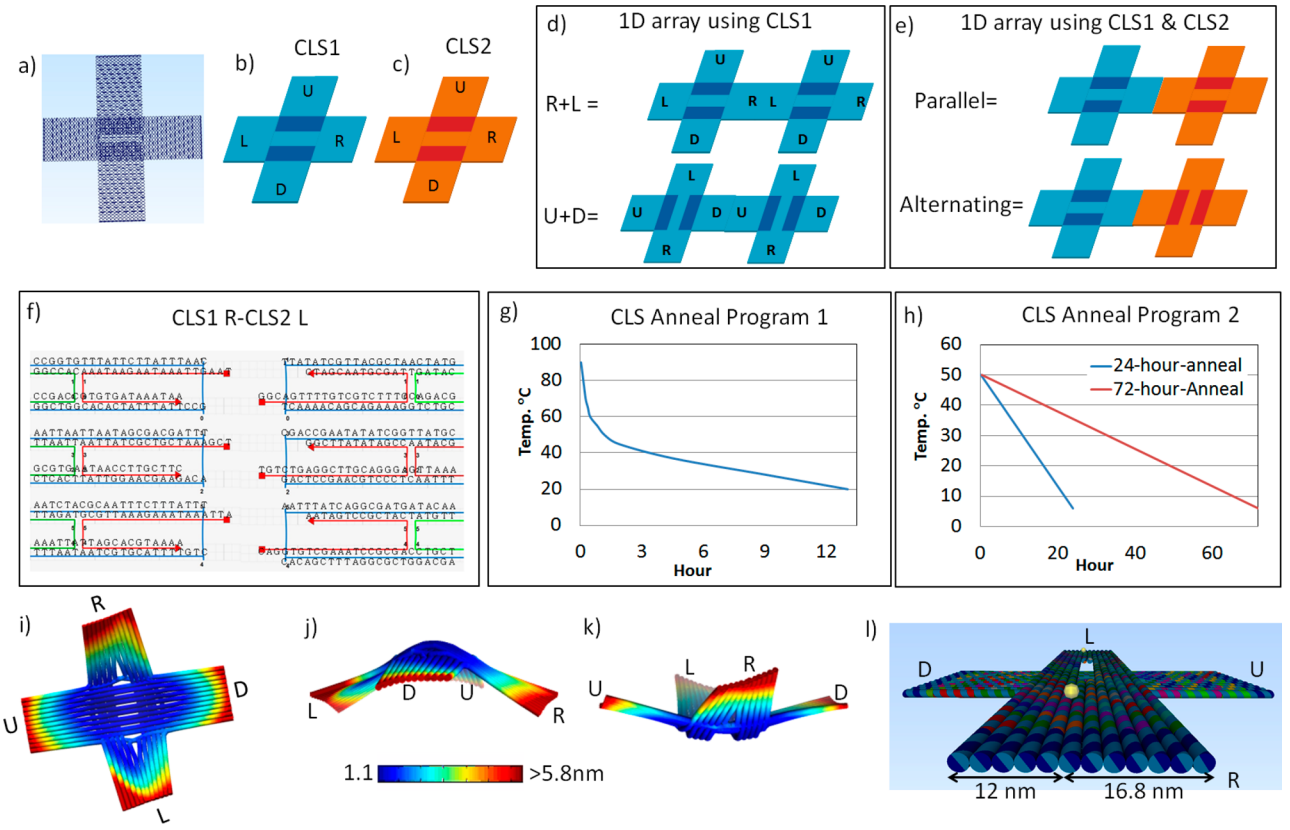

Figure 1. (a) The cross structure with central overlapped region. (b, c) The two kinds of CLSs used in this study are drawn in blue (CLS1) and in orange (CLS2) throughout the manuscript for clarity. (d) An illustration of two kinds of connections used to generate two isomeric forms of 1D arrays from CLS1 tiles. (e) The two kinds of connection used to form 1D origami arrays of finite length from two CLS with different sequences. (f) caDNAno design showing 6 of the 12 helixes connecting the right arm of CLS1 to the left arm of CLS2. Blue lines are the M13 scaffold, and the red lines are the end staples including their sticky ends, which are the three extra bases at the 5′ end that complement the scaffold on the arm of the other cross. (g) Plot of temperature vs time for the first anneals. The CLS anneal program 1 is used to prepare the CLS tiles. (h) The 2nd anneal uses program 2 to assemble the 1D array by dropping temperature from 50 to 6 °C over a 1-day or a 3-day-anneal. (i) CanDo 3D prediction of CLS tile structure. (j) Side view of CLS tile. The overall structure of CLS bends downward. (k) Inverted CLS, which is the structure of tiles 3, 4, 7, and 8 in the alternating design. (l) a close up view drawn using Maya showing the location of the streptavidin on CLS1. The streptavidin is shifted 2.4 nm away from the middle line.

under well-defined conditions.[17−20] As the complexity of constructs and the density of independent surface bound species on these increases, there will be increased pressure to determine the kinetics of assembly, errors in assembly, and mechanisms for errors in assembly. In contrast to the current solution phase assembly approach, which is most amenable to post-assembly characterization, assembly on immobilized 1D array systems can provide the opportunity for real-time, in situ characterization of the growth process via high-speed optical and AFM monitoring systems. Ideally, these systems would consist of a large number of serially arranged "identical" platforms with identical relative orientations and, to the extent controllable, present identical assembly or receptor sites to the assembly solution. The value of a system with nearly atomic placement precision over micrometer distances will only be realized when the ability to characterize the assembly process, and therefore assembly error processes, becomes commonplace.

1.4. Expanding Dimensionality

The second driver for the development of 1D systems is the hypothesis that large error rates in finite systems of higher dimensionality can only be avoided through hierarchical assembly that is sequentially directed, enabled, or gated. In this approach, rather than generating a design for a 3D system that enables one to mix all of the components simultaneously and allow self-assembly processes to generate a "bulk" structure, one posits that each step in the assembly process must be controlled and controllable, such that the step is allowed to proceed to completion before the next step in assembly is enabled.[21] While this modular and serial approach is not as intellectually appealing as a one homogeneous reaction solution approach, particularly in view of the kinetic burden step completion implies, it may be argued that assembly even in 2D can be readily foiled through errors in incorporation of building blocks, which then lead to failures in propagation of the growth motif.[22−24] This Account explores the high yield generation of finite 1D systems from a building block motif that is thermally robust, highly reproducible, and well suited for incorporation into higher dimensional finite systems.

2. CROSS-LIKE STRUCTURE (CLS) ORIGAMI AS A STANDARDIZED BUILDING BLOCK

The four-armed CLS core motif is shown in Figure 1a. This structure was originally designed and used successfully by W. Liu et al. to generate nonfinite 2D arrays of origami.[23] As will be discussed in more detail later, systems can be designed that will assemble with no preprogrammed termination, which

dx.doi.org/10.1021/ar400330y | Acc. Chem. Res. 2014, 47, 1750−1758

therefore contain an indeterminate number of building blocks and might be termed semi-infinite or nonfinite, as opposed to systems that contain a programmed number of blocks, which may be termed finite. This building block is quite amenable to both types of structures. The core motif is assembled from the 7249 base M13 scaffold and 201 short staple sequences, which includes 177 core staple sequences and 24 edge staple sequences. The CLS is composed of an overlay of two rectangular plate like structures, one vertical, with up and down arms, and one horizontal, with arms to the left and right. Each arm is composed of 12 helixes. The horizontal plate has a window region in the center. As shown in Figure 1a, a square, central region is double-layered when the two plates are overlapped, with the exception of the window area. This window in the center of the double layer has the appearance of an equal sign when imaged using AFM, which enables one to easily discern the orientation of the CLS (up and down vs left and right).

There are several unique factors that recommend this four armed CLS structure for use in 1D and 2D systems and therefore for use as a standard building block for generation of macrostructures, both finite and semi-infinite. One of the most important aspects is that this motif provides an equivalent mechanism for growth in two perpendicular it presents the ends of helical domains at the ends of each arm. This equivalence of binding interactions along both orthogonal directions means that association and dissociation kinetics will be, to a first approximation, isotropic, leading to the possibility of equal growth rates in two dimensions. Although within the footprint of the design the system has a very high density of staples, and therefore not only high mechanical stability but also a high density of binding sites for surface modification, the cross motif is most amenable to generation of a non-space-filling tiling. Because the arms bind end to end, square voids exist along the diagonal direction. This void space may find future use as "via" space, providing access to the substrate or providing channels endowing the system with porosity. This construct, as with most current origami, does not use the M13 plasmid sequence completely, leaving a remainder portion of the sequence, a tail, uncomplemented and dangling, usually from the edge of the structure. For single origami systems, this does not present a problem. However, for systems that are designed to pack, this excess material at least can provide a kinetic barrier to assembly (sterics) or at worst can interfere with assembly, destroying the coherence of the assembly. However, in the CLS, this tail region is designed to be positioned in the void space, where it cannot interfere with assembly.

While optical methods, particularly FRET (fluorescence resonant energy transfer) have provided insight into the dynamic structure of particular locations of interest in finite origami objects, for example, the closure of an origami box,[21] extended distance scales require the application of other methods. In order to obtain a more direct understanding of the principal structural features that may contribute to any observed differences in persistence lengths for different structures, the program CanDo was used to provide a predicted 3D structure for the CLS tile (Figure 1i). CanDo, developed by M. Bathe et al., is an important program for evaluating origami structures[25,26] and is much more accessible than cryo-EM,[27] a direct imaging tool. The plot is color-coded using the values computed for root-mean-square thermal fluctuations. This prediction reveals that the overall structure of the CLS as modeled is significantly distorted, with the left and right arms departing most from planarity. In addition to this bending, deformation at the end of each of the four arms can also be observed and may be partially explained by the design using a helix twist of 33.75°/bp or 10.67bp/turn, as opposed to the standard B-form DNA, which has a 34.6°/bp or 10.4 bp/turn pitch.[28,29] If the twist angle per construct is small, the arrays will flatten on binding to a solid substrate and the AFM images will not reflect this twisting. If the twist angle is high and the 1D array length spans greater than a 180° rotation, then one may anticipate observing folded arrays via AFM.

3. TYPES OF INTERORIGAMI JUNCTIONS

3.1. Geometrical

Shortly after the invention of origami, Rothemund et al. demonstrated the significance of helical stacking in origami−origami interactions.[16] While origami do not tend to stack on top of each other and they do not tend to align alternating to the directions of the helices, strong interactions between edges of an origami presenting blunt helical ends can generate unintended multiple origami parallel along the helical direction. This interaction is so powerful that it has been suggested as a sole binding force for origami−origami supramolecular constructs.[30−33] In strong contrast to the majority of origami structures published to date, in the cross origami design, this stacking energy contribution adds stability to the interorigami interactions in two orthogonal directions.

3.2. Sticky End−Sticky End

In the original design by W. Liu et al., the ends of each of the four arms of the core of the CLS construct were extended using two sets of 5 bp overhangs.[23] This resulted in the equivalent of two cross constructs, which were entirely different in their recognition sequences, even though the cores were exactly the same. An in-depth study of this approach to the generation of 1-D arrays has been recently reported.[17] Such use of overhang sequences minimizes the expense and complexity of assembly while providing a path to design of systems with a potentially large number of unique tiles.

3.3. Sticky End−Scaffold

We have taken an alternative approach to generate two different CLSs used in the majority of our 1D studies. CLS1 and CLS2 are represented by the blue cross and orange cross in Figure 1b,c. The structure and design of the two crosses are identical. The difference is that each of the folding designs starts at a different location on the M13 plasmid, which requires the sequence of every staple to be completely different. Instead of utilizing the geometrical arrangement of blunt-end stacking interactions[17,30] or pairs of sticky ends,[23] the connection between the CLSs is made by base pairing from sequences at the end of each arm, which have three extra bases that are complementary to the m13 plasmid scaffold of the adjacent CLS arm. In other words, a connection is made through 36 weak single base interactions per arm. To clarify, a screenshot of a structure map generated using caDNAno of half of one arm, explicitly showing these interorigami bindings, is shown in Figure 1f. caDNAno is an excellent open-source program that can be used to design 3D DNA-origami shapes constrained to a square or honeycomb shaped framework or lattice.[34,35] This figure presents the first six helixes connecting the right arm of CLS1 and the left arm of CLS2. This binding results in the alignment of the "equal signs" and is termed a parallel segment

dx.doi.org/10.1021/ar400330y | Acc. Chem. Res. 2014, 47, 1750−1758

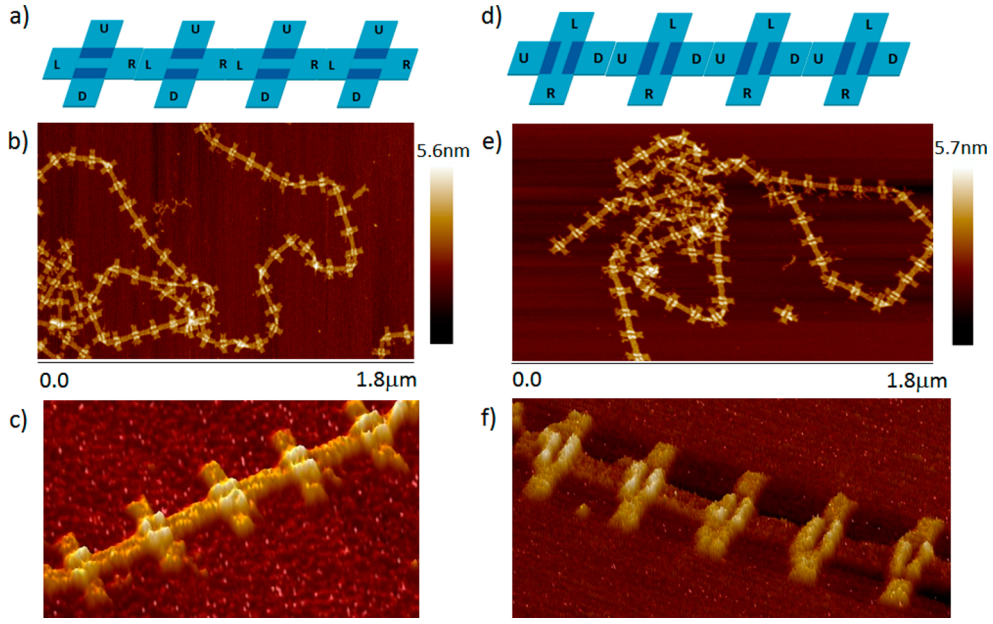

Figure 2. (a) Schematic illustration of one type of 1D array forming pattern made by connecting CLS1 blocks using R and L arms. The landmark equal (=) sign is then parallel to the long axis of the array. (b) AFM image of a long 1D parallel array. (c) High resolution AFM image. (d) Schematic view of the "perpendicular" type of 1D array formation pattern generated by connecting U and D arms of CLS1 blocks. The equal signs are all perpendicular to the long array direction. (e, f) AFM images of this type of 1D array.

(Figure 1e). Combining a top or down arm with a left or right arm results in alternating segment (Figure 1e). Unique linkages between any two arms can be programmed through these 36 base complementary matches. For arms where binding is not desired, these three extra bases are replaced with five thymines, a technique previously suggested in the literature.[16,17,36] These five thymines prevent nonspecific binding and interfere with or disrupt the $\pi-\pi$ stacking interactions.

4. METHODS AND PROTOCOLS OF ASSEMBLY

Two sources were used for the DNA components necessary to assemble CLS. The single-stranded M13mp18 DNA plasmid scaffold was purchased at a concentration of 1.00 μg/μL from Bayou Biolabs, and all of the staple strands and sticky-end strand sequences were obtained from Integrated DNA Technologies Inc. at a 25 nmol synthesis scale and in standard desalted purified form. In a generic preparation, a solution composed of a mixture of staple strands, designed sticky ends, and M13mp18 ssDNA plasmid is brought to a volume of 50 μL using CLS buffer (1× Tris-acetate-EDTA (TAE) buffer with 12.5 mM of $MgCl_2$). The final concentration of ssDNA plasmid in the solution is 10 nM, and the molar ratio of the ssDNA plasmid to each of the other strands is 1:5. To first form individual CLS blocks, the solution with the designed sticky ends appropriate for one construct is first annealed in a slow cooling process, dropping the temperature from 90 to 20 °C over a 13 h period.

This annealing program is shown in Figure 1g. Equal amounts of blocks are then mixed together and annealed from 50 to 6 °C for the formation of the finite arrays. Arrays resulting from a 1-day and a 3-day second anneal (Figure 1h) were compared and are discussed in the following section.

Because we frequently observe "failure products", it is useful to determine whether the incorporated block is the correct type by marking one of the two structures. Streptavidin has a long history of use as a marker in DNA nanotechnology[37] because the streptavidin–biotin complex has one of the highest noncovalent binding strengths in nature, with an associated free energy of 18 kcal/mol.[38−40] In order to make it easier to identify the blocks, one or two arms of the CLS can be modified with two closely spaced biotinylated staples during individual CLS assembly, then labeled through binding with streptavidin as a high contrast marker before imaging with AFM.[41−44] For example, a single streptavidin marker on one arm enables us to identify the CLS1 components of the array and their orientation along all three axes. To break the symmetry of the CLS, two biotinylated staples were positioned between the seventh and the eighth helix of the 12 helixes in the right arm counting from the "up arm" as shown in Figure 1l. Using streptavidin coding in this manner, we can easily identify whether an array block or an entire array is facing up or facing down.

5. GENERATING 1D STRUCTURES

The generation of two broad types of 1D structures is enabled by the CLS origami motif. One is an "infinite" array, which is a concatenated origami polymer of indeterminate length resulting from a single solution reaction. The other is a finite array, composed of distinct origami elements designed to generate a predetermined sequence of elements through self-assembly.

5.1. Nonfinite 1D Array

Two different designs, one termed parallel and another named perpendicular, are represented in Figure 2a,d. The design of these 1D arrays both begin by considering edge modifications of the CLS1 core. In the parallel design, we connect 12 helixes of the right arm of CLS1 via 3 nt long overhanging sticky ends on staples of the left arm of the neighboring CLS1 as shown in Figure 1d as R + L. The perpendicular type array was formed by connecting U and D arms between adjacent origami (Figure 1d; U + D). AFM imaging indicates that both designs yield long 1D arrays of various lengths when annealed using, for example, CLS anneal program 1 (Figure 1g).

dx.doi.org/10.1021/ar400330y | Acc. Chem. Res. 2014, 47, 1750−1758

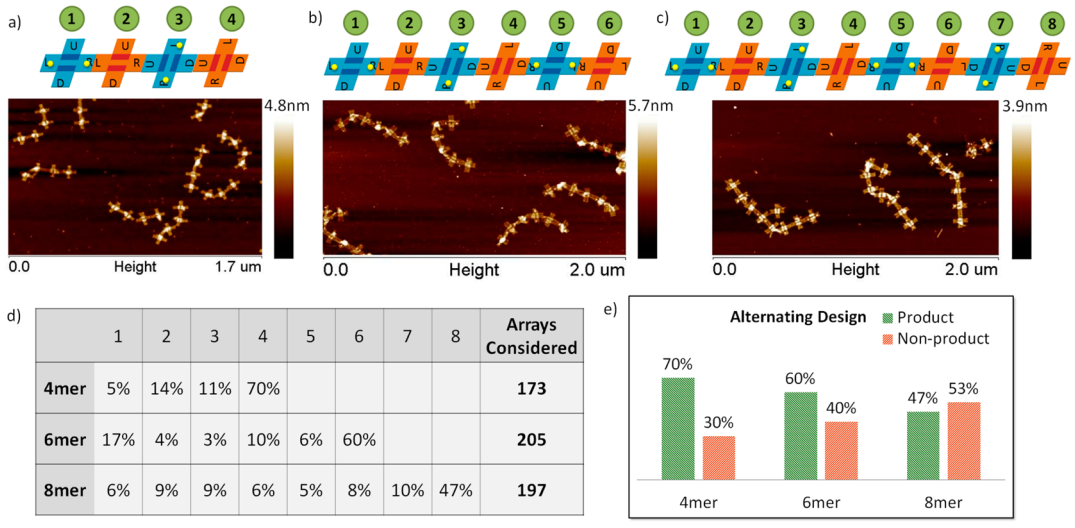

	1	2	3	4	5	6	7	8	Arrays Considered
4mer	5%	14%	11%	70%					173
6mer	17%	4%	3%	10%	6%	60%			205
8mer	6%	9%	9%	6%	5%	8%	10%	47%	197

Figure 3. Illustrations and AFM images of CLS array for the (a) 4mer, (b) 6mer, and (c) 8mer of the alternating design. (d) Formation statistics for each type of array. (e) Histogram representing the yield. Full-length arrays were counted as products; all other origami assemblies are represented as nonproduct.

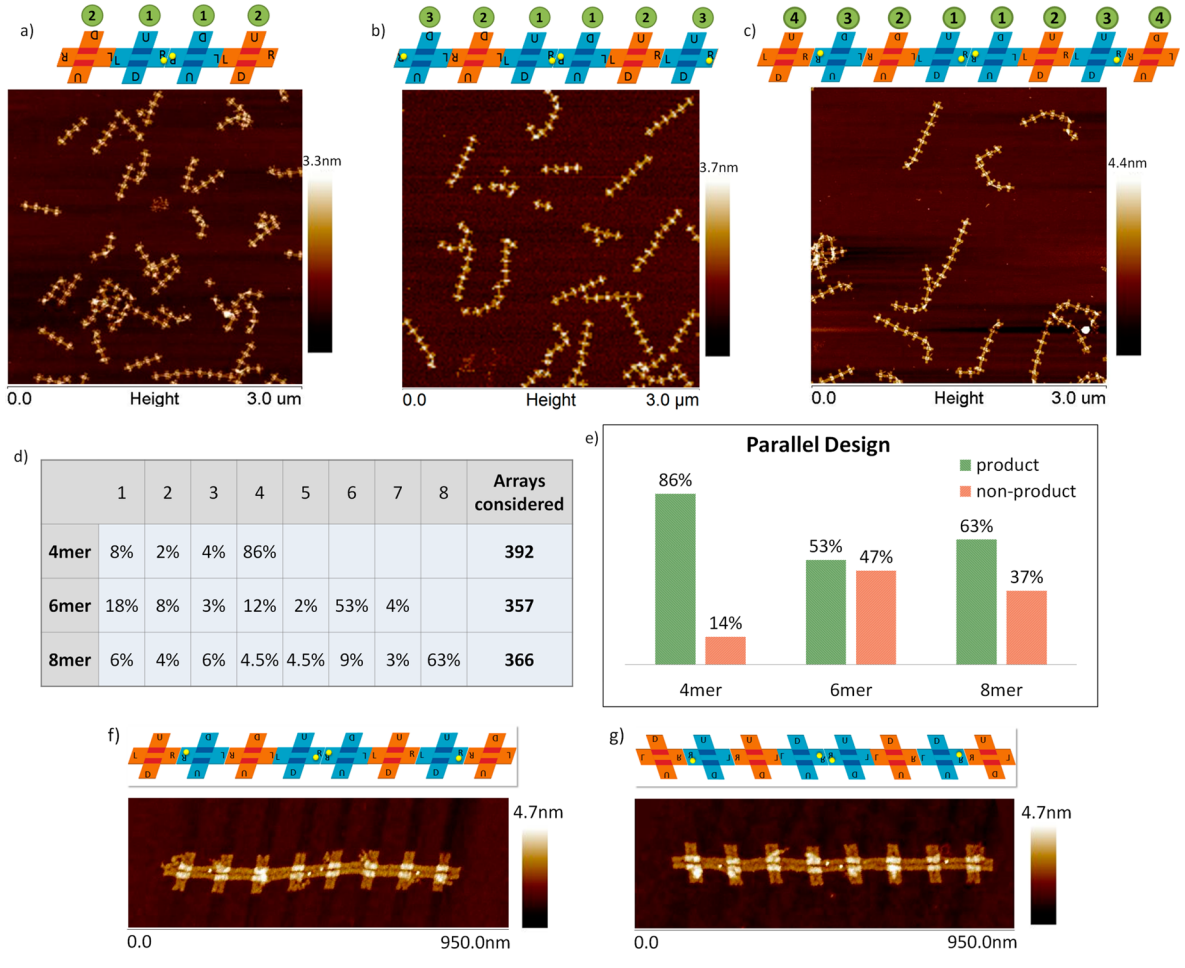

	1	2	3	4	5	6	7	8	Arrays considered
4mer	8%	2%	4%	86%					392
6mer	18%	8%	3%	12%	2%	53%	4%		357
8mer	6%	4%	6%	4.5%	4.5%	9%	3%	63%	366

Figure 4. Illustrations and AFM images of CLS arrays with the parallel design for the (a) 4mer, (b) 6mer, and (c) 8mer. (d) The statistics for formation of all parallel arrays. (e) Histogram of yields. Full-length arrays were counted as products, and all other origami objects were counted as nonproduct. (f) The parallel form 8mer as designed, with top side facing up. The streptavidin label appears on the right arm of CLS1 shifted slightly below the centerline toward the down arm. (g) An upside-down parallel 8mer; streptavidins display mirror symmetry pattern.

5.2. Finite 1D Array

5.2.1. Alternating Design. The first of two design approaches that we have employed to generate origami arrays of specific lengths is called the alternating design. In this design, two CLSs, each with a different core sequence, alternate to form the array (shown in Figure 3a,b,c). By rotating the CLS

dx.doi.org/10.1021/ar400330y | Acc. Chem. Res. 2014, 47, 1750−1758

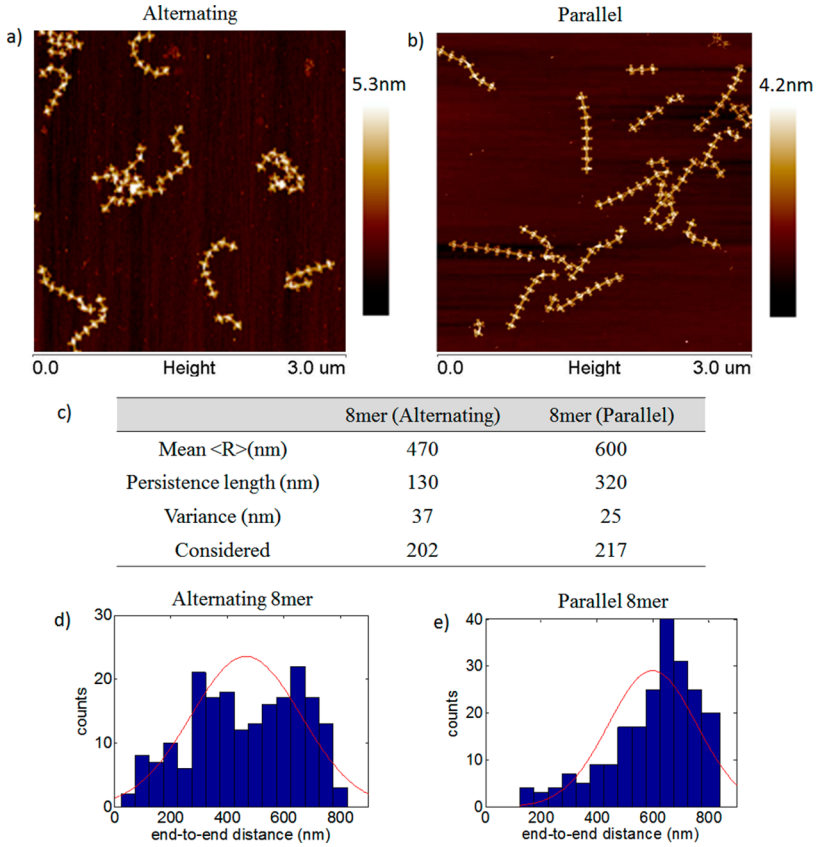

	8mer (Alternating)	8mer (Parallel)
Mean <R>(nm)	470	600
Persistence length (nm)	130	320
Variance (nm)	37	25
Considered	202	217

Figure 5. AFM images of 8mer of (a) alternating and (b) parallel origami arrays. (c) The calculated persistence length values of arrays. (d, e) The distribution *R* of alternating and parallel 8mer arrays, respectively.

90° clockwise in each successive insertion into the array sequence, the four arms of both origamis are combined to create seven different CLS-to-CLS connections. Due to the 5′ to 3′ direction of the scaffold sequence, this alternating design can only be achieved by flipping tiles 3, 4, 7, and 8 upside down while tiles 1, 2, 5, and 6 remain facing up. The uniqueness of each junction design enables us to control the orientation of each CLS and the order of the CLS in the array. To provide assistance in process development, one pair of biotins was used to label the right and left arms of CLS1 in this alternating design.

Progressive steps along the self-assembly path of this design were examined by synthesizing the 4mer, 6mer, and 8mer arrays and using AFM to investigate the yield. Equal volumes of 10 nM solutions of each building block were mixed and annealed using the 3-day anneal program. A reflection of the robust nature of this building block motif, consistent with the reported observations of Liu,[23] the 50 °C annealing temperature does not appear to disrupt the staples at the edges, which are important in selective adhesion. Almost 200 of each type of array (4mer, 6mer, and 8mer), were evaluated in order to obtain the histogram shown in Figure 3d. The 4mer, 6mer, and 8mer were found to have yields of 70%, 60%, and 47% for the completely formed arrays, respectively. The longer the array was, the lower the yield, as might be expected since the increased complexity provides an increasing number of failure modes. In parallel with the 3-day anneal, a 1-day assembly (termed a second anneal in Figure 1h) was also performed. The observed yields were essentially the same, which suggests that kinetic control rather than equilibrium factors determine the error product distribution.

5.2.2. Parallel Design. The arrays generated with the parallel pattern (all = signs parallel along the long array direction) are much less complex in design, having a 2-fold rotational axis perpendicular to the array plane. Two identical CLSs bind to each other at the center of the array (Figure 4a,b,c), so only four different blocks are required to form the 8mer shown in Figure 4c. Experiments with this array design had as objectives not only achieving high yield of origami arrays of specific lengths but also experimentally determining whether there were differences in the binding characteristics of the arms not readily apparent in the design. This is important because the best building block design will be one that produces an origami array that is naturally resistant to spiral twisting in solution and kinking upon drying. Origami arrays based on this design were assembled, with example images shown in Figure 4.

The arrays are generated by mixing together equal volumes of 10 nM solutions of preannealed building blocks and annealing the resulting solutions from 50 to 6 °C over 24 h. This parallel design produces yields of 86% and 63% for the 4mer and 8mer, which are significantly higher than the yields obtained with the alternating design. However, the 6mer suffered from a lower yield than expected from this trend. The relatively high failure rate can be ascribed to the apparent stability of monomer, dimer, and tetramer structures.

The two different component blocks used in the design of the arrays discussed above appear identical in AFM images. However, for identification purposes, in addition to the "equal sign", we used streptavidin as a high *Z* and therefore high contrast marker on the surface. Not only does this enable us to differentiate CLS1 from CLS2, but this marker also can be used to determine whether CLS1 is right side up or upside down.

dx.doi.org/10.1021/ar400330y | *Acc. Chem. Res.* 2014, 47, 1750−1758

Only one pair of biotins, positioned on only the right arm, was required for labeling in this parallel design (Figure 4f,g).

6. STIFFNESS AND PERSISTENCE LENGTH

Even a consideration of the few images provided in Figures 3 and 4 seems to indicate that the parallel pattern provides structures with considerably less bending and kinking of the observed arrays. This significantly improved linearity of the arrays increases their potential to serve as substrates or structural components or spacers for organizing other nanomaterials for applications. We considered 202 alternating 8mer arrays and 217 parallel 8mer arrays to obtain the end-to-end distance mean values, $\langle R \rangle$, standard deviations, and mean square, $\langle R^2 \rangle$ for both designs (Figure 5c). The parallel design has a longer end-to-end distance vector, and the distance distribution, represented as a histogram plotted with a bin size of 50 nm, suggests that the parallel structure has one major mode (closer to a single Gaussian distribution approaching the full length of the array). According to the ideal chain model, R should be normally distributed. A Gaussian curve was therefore plotted (red line) for comparison in both histogram plots (Figure 5d,e) based on the mean value and standard deviation tabulated in Figure 5c. We used one of the special cases of the ideal chain, the worm-like chain (WLC), to model the 8mer. Unlike the ideal chain, which is only flexible between discrete segments, the WLC model considers the segments to be continuously flexible. The 2D Kratky−Porod model relates the mean square end-to-end distance with the persistence length via eq 1:

$$\langle R^2 \rangle = 4pL[1 - 2p(1 - e^{-L/(2p)})/L] \quad (1)$$

where R is the of end-to-end distance, the angle brackets denote the average value, p is the persistence length, and L is the contour length.[45−47] If we assume that a single CLS is approximately 92 nm from end to end, then the contour length of a single 8mer is 736 nm. The persistence length of the alternating arrays is then 130 nm, and p for the parallel 8mer arrays is 320 nm. These values are significantly lower than those found for origami tubes.[43] While qualitative, because the model is sequence independent, the departures from planarity observed in the CanDo model (Figure 1i−k) represent departures from the WLC model in which bond directions should be random rather than biased. In the alternating design, which consists of up to 50% blocks with the "perpendicular" orientation, significant departures from linearity are observed in Figure 3a−c coincident with folds located at origami blocks. These folds result in the formation of the small R structures represented in the plot in Figure 5d. Such folds are not frequently observed for the parallel structures, which do not contain blocks with the perpendicular orientation. We note that Liu's 2D origami crystal design included rotational randomization at each of the two types of lattice sites, to great effect.[23] For the rather short, flat chains studied here, departures from planarity and twists in the building block unit can significantly impact the observed persistence length. This bias represents the greatest, but not the only departure of an anisotropic origami design from the model.[43]

7. CONCLUSIONS

This Account reviews efforts directed toward the high yield fabrication of finite 1D multiorigami arrays. For the longest finite parallel design arrays considered, the 8mer, the yield was found to be 63%. From a materials use perspective, on the order of 77% of all individual origami counted were incorporated into the 8mer product. While there are certainly many arrays with errors, more than half of the observed objects are the fully formed ones. Each linkage in the array is encoded by its unique sequence. These links not only provide a path toward product formation, but also can function as multifaceted error nodes, with potential to act as kinetic traps by creating error junctions, which can inhibit further growth and product formation. Higher purity materials may be achieved either through a separation process, assuming no spontaneous breaking or via yield optimization. Efforts to produce higher yields will require identification of these error generating trap states and the minimization of their impact via optimization of multiple unique linkage sequences. The parallel design displayed higher yield and a higher persistence length than the alternating design. One factor possibly contributing to the higher yield is the difference in the number of different junctions required. Only four different junctions were required to form the 8mer parallel array. In contrast, in the alternating design the scaffold sequences for each arm are used to encode two different junctions, one with a "right side up" partner, and one with an upside down partner (Figure 3c). This can lead to error junctions since there can be competition for scaffold sites by more than one type of tile. Such competitive binding at junctions may present important kinetic trap states.

Addressing several additional challenges will speed the adoption of origami as a substrate for more complex molecular machines or circuits. "Standard elements" with high structural rigidity, designed for ready integration into large nanosystems, immobilized and aligned on technological substrates such as silicon, must be made available to the engineering community. Such immobilization is a necessary precursor to the generation of electrical, optical, chemical, and mechanical connections to working nanosystems. The foundations for relatively long finite 1D arrays now exist. Motivated by the success of Liu,[23] in producing nonfinite 2D arrays from CLSs, experiments directed toward solution phase assembly of finite two-dimensional systems seeded by these finite 1D arrays are currently ongoing in our laboratories.

■ AUTHOR INFORMATION

Corresponding Author

*Michael Norton. E-mail: norton@marshall.edu.

Funding

We acknowledge the following grants to support this research: ARO awards W911NF-08-1-0109, W911NF-09-1-0218, and W911NF-11-1-0024 and NSF Cooperative Agreement Number EPS-1003907.

Notes

The authors declare no competing financial interest.

Biographies

Dr. Tsai-Chin Wu has a background in physics and obtained her Ph.D. in Bioengineering from the University of Illinois at Chicago in 2012. During her Ph.D. research, she began exploring the potential of utilizing DNA molecules and nanoparticles to build sensors at the nanometer scale. As a postdoctoral fellow in the Department of Chemistry at Marshall University, she is expanding her knowledge and experience in microfluidics and self-assembly of DNA structures.

Dr. Masudur Rahman received his Ph.D. in Environment & Life-science Engineering from Toyohashi University of Technology (TUT), Japan, in 2007 as a Monbukagakusho Scholar. He developed a quasi-real-time airborne pathogen detection system during his postdoctoral research at TUT. At Marshall University, his research is focused on connecting bottom-up methods of patterning with top-down approaches for optoelectronic sensing by developing micro- or nanofabrication systems based on DNA nanostructures and interference lithography systems for single molecule localization.

Dr. Michael Norton obtained his Ph.D. in Solid State Chemistry from Arizona State University in 1982, working in the area of two-dimensional materials. As a NRC postdoctoral researcher, he worked briefly in the area of oxide materials at the Naval Weapons Center at China Lake, California. As an assistant professor at the University of Georgia, he developed methods for the electrochemical growth of superconducting oxide superlattices. In his career at Marshall University, his studies have focused on soft matter structures, including DNA based nanostructures, with emphasis on the fabrication and characterization of electro-optical nanoarchitecture for sensing applications.

REFERENCES

(1) Seeman, N. C. DNA nanotechnology: Novel DNA constructions. *Annu. Rev. Biophys. Biomol. Struct.* **1998**, *27*, 225−248.
(2) Seeman, N. C. An overview of structural DNA nanotechnology. *Mol. Biotechnol.* **2007**, *37*, 246−257.
(3) Zadegan, R. M.; Norton, M. L. Structural DNA nanotechnology: From design to applications. *Int. J. Mol. Sci.* **2012**, *13*, 7149−7162.
(4) Zhang, G.; Surwade, S. P.; Zhou, F.; Liu, H. DNA nanostructure meets nanofabrication. *Chem. Soc. Rev.* **2013**, *42*, 2488−2496.
(5) Zhao, Y. X.; Shaw, A.; Zeng, X.; Benson, E.; Nystrom, A. M.; Hogberg, B. DNA origami delivery system for cancer therapy with tunable release properties. *ACS Nano* **2012**, *6*, 8684−8691.
(6) Schüller, V. J.; Heidegger, S.; Sandholzer, N.; Nickels, P. C.; Suhartha, N. A.; Endres, S.; Bourquin, C.; Liedl, T. Cellular immunostimulation by CpG-sequence-coated DNA origami structures. *ACS Nano* **2011**, *5*, 9696−9702.
(7) Douglas, S. M.; Bachelet, I.; Church, G. M. A logic-gated nanorobot for targeted transport of molecular payloads. *Science* **2012**, *335*, 831−834.
(8) Liu, X.; Xu, Y.; Yu, T.; Clifford, C.; Liu, Y.; Yan, H.; Chang, Y. A DNA nanostructure platform for directed assembly of synthetic vaccines. *Nano Lett.* **2012**, *12*, 4254−4259.
(9) Arora, H. C.; Jensen, M. P.; Yuan, Y.; Wu, A.; Vogt, S.; Paunesku, T.; Woloschak, G. E. Nanocarriers enhance doxorubicin uptake in drug-resistant ovarian cancer cells. *Cancer Res.* **2012**, *72*, 769−778.
(10) Endo, M.; Yang, Y.; Sugiyama, H. DNA origami technology for biomaterials applications. *Biomater. Sci.* **2013**, *1*, 347−360.
(11) Zheng, M.; Jagota, A.; Semke, E. D.; Diner, B. A.; McLean, R. S.; Lustig, S. R.; Richardson, R. E.; Tassi, N. G. DNA-assisted dispersion and separation of carbon nanotubes. *Nat. Mater.* **2003**, *2*, 338−342.
(12) Surwade, S. P.; Zhou, F.; Wei, B.; Sun, W.; Powell, A.; O'Donnell, C.; Yin, P.; Liu, H. Nanoscale growth and patterning of inorganic oxides using DNA nanostructure templates. *J. Am. Chem. Soc.* **2013**, *135*, 6778−6781.
(13) Surwade, S. P.; Zhao, S.; Liu, H. Molecular lithography through DNA-mediated etching and masking of SiO_2. *J. Am. Chem. Soc.* **2011**, *133*, 11868−11871.
(14) Deng, Z.; Mao, C. Molecular lithography with DNA nanostructures. *Angew. Chem., Int. Ed.* **2004**, *43*, 4068−4070.
(15) Kershner, R. J.; Bozano, L. D.; Micheel, C. M.; Hung, A. M.; Fornof, A. R.; Cha, J. N.; Rettner, C. T.; Bersani, M.; Frommer, J.; Rothemund, P. W.; Wallraff, G. M. Placement and orientation of individual DNA shapes on lithographically patterned surfaces. *Nat. Nanotechnol.* **2009**, *4*, 557−561.
(16) Rothemund, P. W. Folding DNA to create nanoscale shapes and patterns. *Nature* **2006**, *440*, 297−302.
(17) Kim, K. N.; Sarveswaran, K.; Mark, L.; Lieberman, M. Comparison of methods for orienting and aligning DNA origami. *Soft Matter* **2011**, *7*, 4636−4643.
(18) Li, Z.; Liu, M.; Wang, L.; Nangreave, J.; Yan, H.; Liu, Y. Molecular behavior of DNA origami in higher-order self-assembly. *J. Am. Chem. Soc.* **2010**, *132*, 13545−13552.
(19) Mangalum, A.; Rahman, M.; Norton, M. L. Site-specific immobilization of single-walled carbon nanotubes onto single and one-dimensional DNA origami. *J. Am. Chem. Soc.* **2013**, *135*, 2451−2454.
(20) Rahman, M.; Neff, D.; Norton, M. L. Rapid, high yield, directed addition of quantum dots onto surface bound linear DNA origami arrays. *Chem. Commun.* **2014**, *50*, 3413−3416.
(21) Andersen, E. S.; Dong, M.; Nielsen, M. M.; Jahn, K.; Subramani, R.; Mamdouh, W.; Golas, M. M.; Sander, B.; Stark, H.; Oliveira, C. L. P.; Pedersen, J. S.; Birkedal, V.; Besenbacher, F.; Gothelf, K. V.; Kjems, J. Self-assembly of a nanoscale DNA box with a controllable lid. *Nature* **2009**, *459*, 73−76.
(22) Yan, H.; Park, S. H.; Finkelstein, G.; Reif, J. H.; LaBean, T. H. DNA-templated self-assembly of protein arrays and highly conductive nanowires. *Science* **2003**, *301*, 1882−1884.
(23) Liu, W.; Zhong, H.; Wang, R.; Seeman, N. C. Crystalline two-dimensional DNA-origami arrays. *Angew. Chem., Int. Ed.* **2011**, *50*, 264−267.
(24) Liu, Y.; Ke, Y.; Yan, H. Self-assembly of symmetric finite-size DNA nanoarrays. *J. Am. Chem. Soc.* **2005**, *127*, 17140−17141.
(25) Bathe, M. Computer-aided engineering for DNA origami (CanDo). http://cando-dna-origami.org/, 2011.
(26) Castro, C. E.; Kilchherr, F.; Kim, D. N.; Shiao, E. L.; Wauer, T.; Wortmann, P.; Bathe, M.; Dietz, H. A primer to scaffolded DNA origami. *Nat. Methods* **2011**, *8*, 221−229.
(27) Bai, X. C.; Martin, T. G.; Scheres, S. H.; Dietz, H. Cryo-EM structure of a 3D DNA-origami object. *Proc. Natl. Acad. Sci. U. S. A.* **2012**, *109*, 20012−20017.
(28) Wang, J. C. Helical repeat of DNA in solution. *Proc. Natl. Acad. Sci. U. S. A.* **1979**, *76*, 200−203.
(29) Dietz, H.; Douglas, S. M.; Shih, W. M. Folding DNA into twisted and curved nanoscale shapes. *Science* **2009**, *325*, 725−730.
(30) Woo, S.; Rothemund, P. W. K. Programmable molecular recognition based on the geometry of DNA nanostructures. *Nat. Chem.* **2011**, *3*, 620−627.
(31) Rajendran, A.; Endo, M.; Katsuda, Y.; Hidaka, K.; Sugiyama, H. Programmed two-dimensional self-assembly of multiple DNA origami jigsaw pieces. *ACS Nano* **2010**, *5*, 665−671.
(32) Endo, M.; Sugita, T.; Rajendran, A.; Katsuda, Y.; Emura, T.; Hidaka, K.; Sugiyama, H. Two-dimensional DNA origami assemblies using a four-way connector. *Chem. Commun.* **2011**, *47*, 3213−3215.
(33) Endo, M.; Sugita, T.; Katsuda, Y.; Hidaka, K.; Sugiyama, H. Programmed-assembly system using DNA jigsaw pieces. *Chemistry* **2010**, *16*, 5362−5368.
(34) Douglas, S. M.; Dietz, H.; Liedl, T.; Hogberg, B.; Graf, F.; Shih, W. M. Self-assembly of DNA into nanoscale three-dimensional shapes. *Nature* **2009**, *459*, 414−418.
(35) Douglas, S. M.; Marblestone, A. H.; Teerapittayanon, S.; Vazquez, A.; Church, G. M.; Shih, W. M. Rapid prototyping of 3D DNA-origami shapes with caDNAno. *Nucleic Acids Res.* **2009**, *37*, 5001−5006.
(36) Ke, Y.; Lindsay, S.; Chang, Y.; Liu, Y.; Yan, H. Self-assembled water-soluble nucleic acid probe tiles for label-free RNA hybridization assays. *Science* **2008**, *319*, 180−183.
(37) Lund, K.; Liu, Y.; Lindsay, S.; Yan, H. Self-assembling a molecular pegboard. *J. Am. Chem. Soc.* **2005**, *127*, 17606−17607.
(38) Green, N. M. Avidin. 4. Stability at extremes of pH and dissociation into sub-units by guanidine hydrochloride. *Biochem. J.* **1963**, *89*, 609−620.
(39) Hyre, D. E.; Le Trong, I.; Merritt, E. A.; Eccleston, J. F.; Green, N. M.; Stenkamp, R. E.; Stayton, P. S. Cooperative hydrogen bond

interactions in the streptavidin-biotin system. *Protein Sci.* **2006**, *15*, 459−467.
(40) Chilkoti, A.; Tan, P. H.; Stayton, P. S. Site-directed mutagenesis studies of the high-affinity streptavidin-biotin complex: contributions of tryptophan residues 79, 108, and 120. *Proc. Natl. Acad. Sci. U. S. A.* **1995**, *92*, 1754−1758.
(41) Wu, N.; Wang, Q.; Zhou, X.; Jia, S. S.; Fan, Y.; Hu, J.; Li, B. Probing tethered targets of a single biomolecular complex with atomic force microscopy. *J. Mol. Recognit.* **2013**, *26*, 700−704.
(42) Busuttil, K.; Rotaru, A.; Dong, M.; Besenbacher, F.; Gothelf, K. V. Transfer of a protein pattern from self-assembled DNA origami to a functionalized substrate. *Chem. Commun.* **2013**, *49*, 1927−1929.
(43) Wang, T.; Sha, R.; Dreyfus, R.; Leunissen, M. E.; Maass, C.; Pine, D. J.; Chaikin, P. M.; Seeman, N. C. Self-replication of information-bearing nanoscale patterns. *Nature* **2011**, *478*, 225−228.
(44) Eskelinen, A. P.; Kuzyk, A.; Kaltiaisenaho, T. K.; Timmermans, M. Y.; Nasibulin, A. G.; Kauppinen, E. I.; Torma, P. Assembly of single-walled carbon nanotubes on DNA-origami templates through streptavidin-biotin interaction. *Small* **2011**, *7*, 746−750.
(45) Wang, T.; Schiffels, D.; Cuesta, S. M.; Fygenson, D. K.; Seeman, N. C. Design and characterization of 1D nanotubes and 2D periodic arrays self-assembled from DNA multi-helix bundles. *J. Am. Chem. Soc.* **2012**, *134*, 1606−1616.
(46) O'Neill, P.; Rothemund, P. W.; Kumar, A.; Fygenson, D. K. Sturdier DNA nanotubes via ligation. *Nano Lett.* **2006**, *6*, 1379−1383.
(47) Feldman, D. Book Review of The theory of polymer dynamics, by M. Doi and S. F. Edwards, the Clarendon Press, Oxford University Press, New York, 1986, 391 pp. Price: $78.50. *J. Polym. Sci., Part C: Polym. Lett.* **1989**, *27*, 239−240.